Chapter 3

Lead-, Zinc-, and Iron-Sulfide Mineralization from Northern Iraq

Ali Ismail Al-Juboury, Waleed S. Shingaly,
Elias M. Elias and Mohsin M. Ghazal

Additional information is available at the end of the chapter

http://dx.doi.org/10.5772/intechopen.72483

Abstract

The samples of the mineralization of Pb-, Zn-, and Fe-sulfides were collected from three localities (Dure, Lefan, in the northern Thrust zone; and Sinjar, in the Foothill zone) in Northern Iraq. The geochemical recognition using X-ray diffraction (XRD) affirms the presence of the ore deposit sulfides (pyrite, sphalerite, galena, smithsonite, and cerussite). The characterization of mineral chemistry using electron microprobe analysis (EMPA) gives a clear and exact percentage of each element in each mineral. Fluid inclusions are mostly liquid H_2O and/or water vapor, which may also contain lesser soluble salts and slightly ore elements. Some fluid inclusions contain CO_2 vapor. This occurrence suggests the presence of two immiscible phases due to boiling at the time of their trapping. They are of epithermal system. The homogenization temperatures and salinities obtained for fluid inclusions can be comparable to those reported for the Mississippi Valley Type (MVT) lead-zinc deposits. It is concluded from the petrographic evidence, fluid inclusions and stable isotope data that lead-zinc mineralization was formed due to deeply circulating high-temperature fluids (brines) within the source basin, or later on by tectonic processes, which possibly contribute in leaching metals from either the diagenesis of host rocks or dewatering of deeper buried siliciclastic beds.

Keywords: mineralization, sulfides, Pb-Zn-Fe, geochemistry, paragenesis, Northern Iraq

1. Introduction

The Northern Iraqi Thrust zone and Foothill zone, where the three studied sections of the present study (Dure, Lefan, and Sinjar) are located, is considered as a good place of mineralization of many ore deposits, especially the lead-, zinc-, and iron-sulfides. This is because the structural, tectonic, and lithologic factors made essentially the highly fractured dolomitized limestones act as host rocks for this mineralization. Few detailed studies have been published

which deal with the ore deposit mineralization in the area. First, Al-Bassam et al. [1] mentioned and studied the presence of lead and zinc sulfides. Then, other studies have been accomplished, but the more recent detailed geochemical investigation and exploration were carried out by Awadh [2, 3] and Shingaly [4]. The present chapter deals with the mineralization of sulfides in the above-mentioned three sections. It is worth to mention that this mineralization in Sinjar area is given for first time in such geochemical point of view. The work is a part of PhD research performed at Mosul University by the second author. The geochemical prospect of this work aims first to document the presence of the mineralization of the sulfide ore deposits in Northern Iraq, and second to elucidate their paragenesis, their source, and the processes responsible for their occurrence through the analysis of data obtained by the techniques of X-ray diffraction (XRD), electron microprobe analysis (EMPA), fluid inclusions, and stable isotopes of ^{13}C, ^{18}O, and ^{34}S.

2. Geology

The area of study had been influenced by Alpine orogeny that affected strongly the northern part of Iraq. During the time from Permian to mid-Cretaceous, the northern to eastern parts of the Arabian plate were subsiding gradually and bordering the Neo-Tethys Ocean [5]. The northern thrust zone on the Iraqi territories is formed to be as a developed ridge at the Arabian plate throughout the Zagros suture formed within the domain of the Neo-Tethys. During the movement of the Arabian plate and Tethys development, the mineralization of ore deposits occurred in the area as documented by Al-Bassam et al. [1], and later on by others as, for example, Awadh [3]. The host carbonate rocks of the ore deposits are represented mostly by fractures and karstified dolomitized limestones of Qamchuqa and Mergi formations (Middle Cretaceous), Bekhme formation (Upper Campanian), marly limestone of Shianish formation (Upper Campanian-Maastrichtian), and Kurra Chine formation (Upper Triassic) [6, 7].

The general geology and locations of the three studied sections (Dure, Lefan, and Sinjar) are illustrated in **Figure 1**.

3. Methodology

Representative samples were analyzed using a Philips X-ray diffractometer (PW3710) scanning from 4° to 60° 2θ. The generator was controlled using Philips PC-APD software. Peak identification was enabled using PDF/ICCD database and quantification using Rietveld analysis using commercial program Siroquant (Sietronics, Australia). Analysis was done at laboratories of the Department of Earth Sciences, Royal Holloway of London University.

Quantitative chemical analyses for selective host and sulfide minerals from the studied lead-zinc deposits were obtained from 10 polished sections (carbon coated) with a Cameca 3-spectrometer electron microprobe at University-College London UCL, UK. A defocused 15–25 μm beam was utilized at an accelerating voltage of 15 kV, a sample current of 15 nA, and a counting time of 10 s.

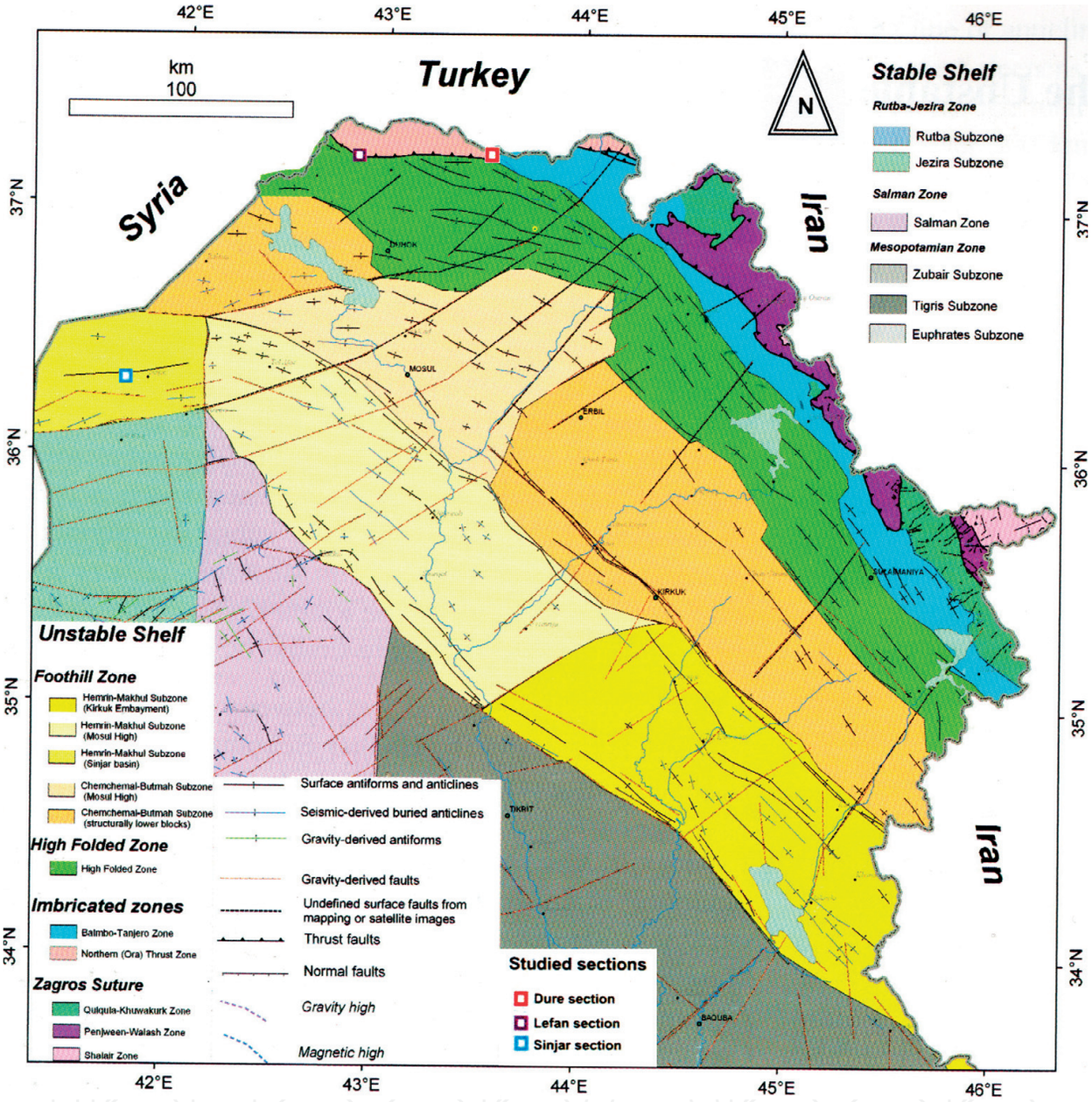

Figure 1. Geology and locations of the studied sections (after Jassim and Goff [8]).

Fluid inclusions were observed under petrographic microscope, and the following parameters were determined by microthermometry: highest temperature of ice melting (last ice melting temperature) (Tm) and homogenization/filling temperature (Th) measurements. Eight double-polished thin sections were prepared from the carbonates (dolomite and calcite) and sphalerite. The microthermometric measurements were taken on a NIKON Labophot-pol microscope mounted with LINKAM THMS-600 and TMS-92 freezing-heating stage and long-distance LW40x objective, in Iran Mineral Processing Research Center (IMPRC), and one sample was also carried out at Geological Engineering Department of Cumhuriyet University in Sivas/Turkey.

Mineral separates for sulfur isotope analysis were acquired by handpicking, and samples were converted to sulfur dioxide gas using a VG Isotech SIRA II mass spectrometer and using laboratory standard gas as a reference to produce true $\delta^{34}S$. The standards employed were the international standards NBS-123 and IAEA-S-3, and the SUERC standard CP-1. Analyses were made at an NERC Isotope Community Support Facility, SUERC, Glasgow, Scotland.

4. Geochemistry of ore deposits

4.1. Recognition

XRD diffractograms definitely illustrated the specific recognition of the sulfides (pyrite, FeS_2; sphalerite, ZnS; galena, PbS; smithsonite, $ZnCO_3$; and cerussite, $PbCO_3$) (**Figure 2**).

4.2. Characterization

The data provided in **Tables 1–3** reveal clearly the chemistry of pyrite, sphalerite, and galena, respectively. The pyrite in **Table 1** composes mainly of 44.7–47.5 wt% Fe and 46.6–55.1 wt% S. The sphalerite in **Table 2** composes essentially of 53.6–69.1 wt% Zn and 31–35.9 wt% S. The galena in **Table 3** composes mainly of 79.9–87.9 wt% Pb and 13.1–14.7 wt% S. Moreover, the calculations of their chemical formulae are given in **Tables 4–6**. The general paragenesis of pyrite, sphalerite, and galena of the three studied sections is illustrated in **Figure 3**. Pyrite is shown to be present in the three localities, where it is more abundant in both main and late stages at both Dure and Sinjar, while it is more abundant in both early and main stages at Lefan.

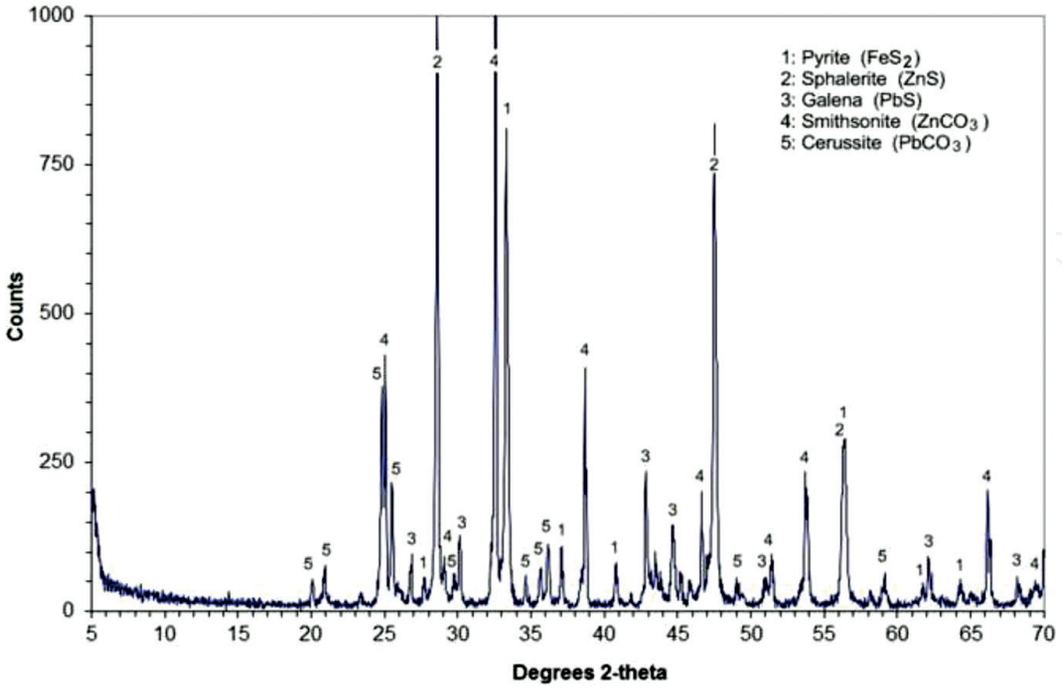

Figure 2. XRD diffractogram for recognition of ore deposits.

	Fe	S	As	Pb	Zn	Ni	Cu	Co	Total	Ore stage
DO 20-1	45.23	51.926	2.695	0.063	0.069	0.0001	0.078	0.003	100.0641	Early
DO 20-2	46.252	52.077	2.247	0.122	0.017	0.0001	0.032	0.003	100.7501	Early
DO 20-3	46.334	52.899	2.225	n.d	0.022	n.d	n.d	n.d	101.48	Early
DO 25-1	46.119	50.26	2.406	0.141	0.16	n.d	0.031	n.d	99.117	Early
DO 25-2	46.583	53.208	1.159	0.056	0.077	n.d	0.047	n.d	101.13	Early
DO 20-1	44.113	51.21	3.803	0.272	1.44	n.d	0.143	0.074	101.055	Main
DO 20-2	44.92	51.35	2.47	0.0931	1.96	0.0001	0.1015	0.003	100.8977	Main
DO 20-3	46.465	49.652	1.805	0.207	0.125	0.0001	0.062	0.002	98.3181	Main
DO 20-4	45.806	52.762	1.253	0.05	1.08	n.d	0.012	0.073	101.036	Main
DO 20-5	46.205	50.849	1.266	1.135	0.013	n.d	n.d	n.d	99.468	Main
DO 20-6	46.526	53.535	1.162	0.059	0.087	n.d	n.d	n.d	101.369	Main
DO 25-1	45.385	54.273	0.058	0.183	0.025	0.0001	0.087	0.1	100.1111	Main
DO 25-2	45.412	54.549	1.039	0.049	0.012	n.d	0.021	0.073	101.155	Main
DO 25-3	45.49	55.141	0.072	0.077	0.021	n.d	0.085	0.099	100.985	Main
DO 25-4	44.939	54.938	0.106	0.107	0.021	0.0001	0.016	0.063	100.1901	Main
DO 26-1	44.745	55.095	0.083	0.088	0.031	0.0001	0.057	0.051	100.1501	Main
DO 26-2	45.29	54.02	1.16	0.028	1.13	n.d	0.0038	n.d	101.6318	Main
DO 26-3	45.59	54.61	n.d	0.1115	1.25	n.d	0.1797	n.d	101.7412	Main
DO 26-4	46.16	53.73	n.d	0.0828	0.6338	n.d	n.d	n.d	100.6066	Main
DO 26-5	46.23	51.06	3.3	0.0489	0.3726	n.d	0.1521	n.d	101.1636	Main
DO 26-6	47.31	53.65	n.d	0.1165	0.232	n.d	0.0269	n.d	101.3354	Main
DO 25-1	47.04	53.75	0.238	0.0066	0.0135	n.d	0.4497	0.002	101.4998	Late
DO 25-2	47.48	52.97	0.0122	0.0673	n.d	n.d	0.0363	n.d	100.5658	Late
DO 25-3	46.22	54.12	0.1334	0.0351	0.6656	n.d	0.0149	0.003	101.192	Late
DO 25-4	46.67	46.66	0.265	0.1967	1.33	n.d	0.0429	n.d	95.1646	Late
DO 25-5	45.79	49.32	2.14	0.1811	1.33	n.d	0.054	n.d	98.8151	Late
DO 25-6	41.85	49.43	1.11	0.2752	5.83	n.d	0.0153	n.d	98.5105	Late
DO 25-7	43.77	50.73	1.96	1.64	1.86	n.d	0.0534	n.d	100.0134	Late
DO 25-8	45.7	49.35	1.89	1.49	2.15	n.d	0.0725	n.d	100.6525	Late
SO 4-1	47.31	54.81	0.003	0.02	0.004	0.04	0	0.002	102.189	Main
SO 4-2	46.12	55.17	0.004	0.004	0.035	0.03	0	n.d	101.363	Main

n.d = not detected.

Table 1. Results of electron microprobe analysis and paragenesis of pyrite in Dure section (DO) and Sinjar section (SO). Elements in wt%.

	Zn	S	Fe	Mn	Cd	Total	Ore stage
DO 26-1	61.11	33.51	5.14	0.016	0.221	99.997	Early
DO 26-2	61.66	33.25	4.23	0.001	0.213	99.354	Early
DO 26-3	61.16	33.2	6.078	0.008	0.227	100.673	Early
DO 26-1	59.81	34.35	6.524	0.011	0.196	100.891	Early
DO 30-1	61.62	32.75	5.514	0.002	0.229	100.115	Main
DO 20-1	62.64	33.53	3.993	0.004	0.236	100.403	Main
DO 20-2	63.2	33.83	3.608	n.d	0.263	100.901	Main
DO 20-3	64.03	32.61	3.797	0.018	0.257	100.712	Main
DO 20-4	63.88	32.52	3.651	n.d	0.226	100.277	Main
DO 25-1	62.39	34.88	2.33	0.003	0.225	99.828	Late
DO 25-2	65.34	34.4	0.81	n.d	0.263	100.813	Late
DO 25-3	65.49	33.55	1.82	n.d	0.277	101.137	Late
DO 25-4	64.49	33.01	2.43	n.d	0.311	100.241	Late
DO 25-5	64.56	33.04	2.62	n.d	0.334	100.554	Late
DO 25-6	69.11	31.01	0.177	n.d	0.244	100.541	Late
DO 25-7	66.83	33.05	0.706	n.d	0.286	100.872	Late
DO 25-8	65.09	33.95	0.968	0.004	0.255	100.267	Late
DO 25-9	65.12	33.69	1.19	0.005	0.26	100.265	Late
DO 30-1	66.22	33.12	0.812	n.d	0.265	100.417	Late
DO 30-2	67.49	32.29	0.129	0.025	0.235	100.169	Late
DO 30-3	66.33	34.08	0.088	n.d	0.279	100.777	Late
DO 30-4	66.29	34.36	0.113	n.d	0.307	101.07	Late
DO 30-5	67.11	33.18	0.052	0.007	0.216	100.565	Late
DO 30-6	68.45	32.31	0.255	0.005	0.263	101.283	Late
DO 30-7	67.65	33.1	0.437	n.d	0.237	101.424	Late
DO 30-9	65.94	33.15	0.259	0.007	0.263	99.619	Late
DO 30-10	66.79	33.28	0.051	0.021	0.272	100.414	Late
LO 10-1	54.5	35.01	9.52	0.001	0.002	99.033	Early
LO 10-2	53.88	35.11	10.14	0.05	0.09	99.27	Early
LO 10-3	53.61	35.91	10.56	0.05	0.09	100.22	Early
LO 18-1	59.1	33.56	7.4	n.d	0.02	100.08	Main
LO 18-2	59.05	33.45	7.45	n.d	0.05	100	Main
LO 18-3	59.41	33.34	7.46	n.d	0.09	100.3	Main
LO 18-4	58.91	33.38	7.82	n.d	0.5	100.61	Main
LO 18-1	62.86	33.51	3.47	0.005	0.5	100.345	Late

	Zn	S	Fe	Mn	Cd	Total	Ore stage
LO 18-2	62.84	33.24	3.49	0.01	0.11	99.69	Late
LO 18-3	62.71	33.56	3.57	n.d	0.19	100.03	Late
SO 4-1	65.1	35.7	0.27	n.d	0.15	101.22	Main

n.d = not detected.

Table 2. Results of electron microprobe analysis and paragenesis of sphalerite in Dure section (DO), Lefan section (LO) and Sinjar section (SO). Elements in wt%.

Sphalerite at Dure is more abundant in the main stage, while at Lefan it is more in both main and late stages. In Sinjar it is recorded only in the late stage with few abundance.

Galena is found more abundant in late stage and less in the main stage at Dure, while it is more in the main stage than in the late stage at Lefan, and no galena is recorded at Sinjar.

Pyrite varies in composition as shown in **Table 4**. At Dure, the pyrite of the early stage has mainly arsenic as traces in Fe-site ($As_{.02–.042}$); other lesser traces are of zinc and copper ($Zn_{.001}$; $Cu_{.001}$). In the main stage, pyrite has relatively more arsenic reaching up to $As_{.06}$, while other

	Pb	S	Fe	Zn	Cd	Total	Ore stage
DO 26-1	86.403	13.612	0.022	n.d	n.d	100.037	Main
DO 26-2	86.635	13.843	0.016	n.d	n.d	100.494	Main
DO 26-3	86.443	13.755	0.018	0.07	n.d	100.286	Main
DO 26-4	87.934	13.154	0.003	0.022	n.d	101.113	Main
DO 25-1	84.73	13.86	0.4338	3.63	0.1672	102.821	Late
DO 25-2	82.75	14.69	0.1514	3.99	0.2513	101.8327	Late
DO 25-3	82.16	14.19	0.3233	3.88	0.1941	100.7474	Late
DO 25-4	82.92	13.86	0.2788	3.15	0.2013	100.4101	Late
DO 25-5	82.52	13.89	0.2209	3.45	0.1777	100.2586	Late
DO 25-6	79.94	13.61	0.7983	5.5	0.1723	100.0206	Late
DO 25-7	86.21	13.86	0.1214	1.36	0.2248	101.7762	Late
DO 25-8	83.11	13.96	0.112	2.13	0.1897	99.5017	Late
DO 25-9	83.16	13.43	0.0881	4.91	0.2263	101.8144	Late
LO 10-1	85.1	13.21	0.04	0.33	n.d	98.68	Main
LO 10-2	84.6	13.22	0.02	0.31	n.d	98.15	Main
LO 10-3	84.03	13.11	n.d	2.34	0.18	99.66	Late

n.d = not detected.

Table 3. Results of electron microprobe analysis and paragenesis of galena in Dure section (DO) and Lefan section (LO). Elements in wt%.

Sample no.	Chemical formula	Ore stage
DO 20-1	Fe(.955 As.042 Zn.001 Cu.001) S2	Early
DO 20-2	Fe(.963 As.035 Cu.001) S2	Early
DO 20-3	Fe(.965 As.035) S2	Early
DO 25-1	Fe(.96 As.04) S2	Early
DO 25-2	Fe(.98 As.02) S2	Early
DO 20-1	Fe(.91 As.06 Pb.002 Zn.03 Cu.003 Co.001) S2	Main
DO 20-2	Fe(.93 As.04 Zn.03) S2	Main
DO 20-3	Fe(.97 As.03) S2	Main
DO 20-4	Fe(.96 As.02 Zn.02) S2	Main
DO 20-5	Fe(.97 As.02 Pb.01) S2	Main
DO 20-6	Fe(.98 As.02) S2	Main
DO 25-1	Fe(.99 As.001 Pb.001 Zn.001 Cu.002 Co.002) S2	Main
DO 25-2	Fe(.98 As.02) S2	Main
DO 25-3	Fe(.99 As.001 Cu.002 Co.002) S2	Main
DO 25-4	Fe(.995 As.002 Pb.001 Co.001) S2	Main
DO 26-1	Fe(.995 As.001 Pb.001 Zn.001 Co.001) S2	Main
DO 26-2	Fe(.96 As.02 Zn.02) S2	Main
DO 26-3	Fe(.973 Pb.001 Zn.023 Cu.003) S2	Main
DO 26-4	Fe(.99 Zn.01) S2	Main
DO 26-5	Fe(.94 As.05 Zn.007 Cu.003) S2	Main
DO 26-6	Fe(.995 Pb..001 Zn.004) S2	Main
DO 25-1	Fe(.988 As.004 Cu.008) S2	Late
DO 25-2	Fe(.999 Cu.001) S2	Late
DO 25-3	Fe(.985 As.002 Zn.012) S2	Late
DO 25-4	Fe(.97 As.004 Pb.001 Zn.024 Cu.001) S2	Late
DO 25-5	Fe(.942 As.033 Pb.001 Zn.023 Cu.001) S2	Late
DO 25-6	Fe(.877 As.017 Pb.002 Zn.104) S2	Late
DO 25-7	Fe(.925 As.031 Pb.009 Zn.034 Cu.001) S2	Late
DO 25-8	Fe(.925 As.029 Pb.008 Zn.037 Cu.001) S2	Late
SO 4-1	FeS2	Main
SO 4-2	Fe(.999 Zn.001) S2	Main

Table 4. Chemical formula of pyrite (calculated from data in **Table 1**).

traces ($Zn_{.001–.104}$, $Pb_{.001}$ $Cu_{.002–.008}$ and $Co_{.001–.002}$) may be found .In the late stage, pyrite has no difference in arsenic content than that of the early stage ($As_{.002–.04}$). The pyrite at Sinjar is very pure (FeS_2); only $Zn_{.001}$ is recorded. At Lefan, no data are available.

Sample no.	Chemical formula	Ore stage
DO 26-1	Zn(.908 Fe.089 Cd.002) S	Early
DO 26-2	Zn(.923 Fe.074 Cd.002) S	Early
DO 26-3	Zn(.894 Fe.104 Cd.002) S	Early
DO 26-1	Zn(.885 Fe.113 Cd.002) S	Early
DO 30-1	Zn(.903 Fe.095 Cd.002) S	Main
DO 20-1	Zn(.928 Fe.069 Cd.002) S	Main
DO 20-2	Zn(.935 Fe.063 Cd.002) S	Main
DO 20-3	Zn(.933 Fe.065 Cd.002) S	Main
DO 20-4	Zn(.935 Fe.063 Cd.002) S	Main
DO 25-1	Zn(.956 Fe.042 Cd.002) S	Late
DO 25-2	Zn(.983 Fe.014 Cd.002) S	Late
DO 25-3	Zn(.966 Fe.031 Cd.002) S	Late
DO 25-4	Zn(.955 Fe.042 Cd.003) S	Late
DO 25-5	Zn(.952 Fe.045 Cd.003) S	Late
DO 25-6	Zn(.995 Fe.003 Cd.002) S	Late
DO 25-7	Zn(.985 Fe.012 Cd.003) S	Late
DO 25-8	Zn(.981 Fe.017 Cd.002) S	Late
DO 25-9	Zn(.977 Fe.021 Cd.002) S	Late
DO 30-1	Zn(.984 Fe.014 Cd.002) S	Late
DO 30-2	Zn(.995 Fe.002 Cd.002) S	Late
DO 30-3	Zn(.996 Fe.002 Cd.002) S	Late
DO 30-4	Zn(.995 Fe.002 Cd.003) S	Late
DO 30-5	Zn(.997 Fe.001 Cd.002) S	Late
DO 30-6	Zn(.993 Fe.004 Cd.002) S	Late
DO 30-7	Zn(.99 Fe.008 Cd.002) S	Late
DO 30-9	Zn(.993 Fe.005Cd.002) S	Late
DO 30-10	Zn(.996 Fe.001 Cd.002) S	Late
LO 10-1	Zn(.83 Fe.17) S	Early
LO 10-2	Zn(.818 Fe.18 Mn.001 Cd.001) S	Early
LO 10-3	Zn(.811 Fe.187 Mn.001 Cd.001) S	Early
LO 18-1	Zn(.87 Fe.13) S	Main
LO 18-2	Zn(.87 Fe.13) S	Main
LO 18-3	Zn(.871 Fe.128 Cd.001) S	Main
LO 18-4	Zn(.862 Fe.134 Cd.004) S	Main
LO 18-1	Zn(.935 Fe.061 Cd.004) S	Late
LO 18-2	Zn(.938 Fe.061 Cd.001) S	Late

Sample no.	Chemical formula	Ore stage
LO 18-3	Zn(.936 Fe.062 Cd.002) S	Late
SO 4-1	Zn(.994 Fe.005 Cd.001) S	Main

Table 5. Chemical formula of sphalerite (calculated from data in **Table 2**).

Sphalerite as shown in **Table 5** is also noticed to have traces of $Fe_{.001–.095}$ and $Cd_{.002–.003}$ in the Zn site of its chemical formula of all stages at Dure, whereas at Lefan, sphalerite has sometimes only $Fe_{.13–.17}$ in its formula in both early and main stages, which is more than that at Dure; in other samples, there is $Cd_{.001–.004}$ that is recorded in all stages. At Sinjar, sphalerite has also $Fe_{.005}$ and $Cd_{.001}$ in the Zn site.

Sample no.	Chemical formula	Ore stage
DO 26-1	Pb(.999 Fe.001) S	Main
DO 26-2	Pb(.999 Fe.001) S	Main
DO 26-3	Pb(.996 Fe.001 Zn.003) S	Main
DO 26-4	Pb(.999 Zn.001) S	Main
DO 25-1	Pb(.863Fe .016 Zn.117 Cd.003) S	Late
DO 25-2	Pb(.858 Fe.006 Zn.131 Cd.005) S	Late
DO 25-3	Pb(.856 Fe.012 Zn.128 Cd.004) S	Late
DO 25-4	Pb(.879 Fe.011 Zn.106 Cd.004) S	Late
DO 25-5	Pb(.872 Fe.009 Zn.116 Cd.003) S	Late
DO 25-6	Pb(.794 Fe.029 Zn.173 Cd.003) S	Late
DO 25-7	Pb(.943 Fe.005 Zn.047 Cd.005) S	Late
DO 25-8	Pb(.917 Fe.005 Zn.074Cd.004) S	Late
DO 25-9	Pb(.836 Fe.003 Zn.156 Cd.004) S	Late
LO 10-1	Pb(.986 Fe.002 Zn.012) S	Main
LO 10-2	Pb(.988 Fe.001 Zn.011) S	Main
LO 10-3	Pb(.916 Zn.081 Cd.004) S	Late

Table 6. Chemical formula of galena (calculated from data in **Table 3**).

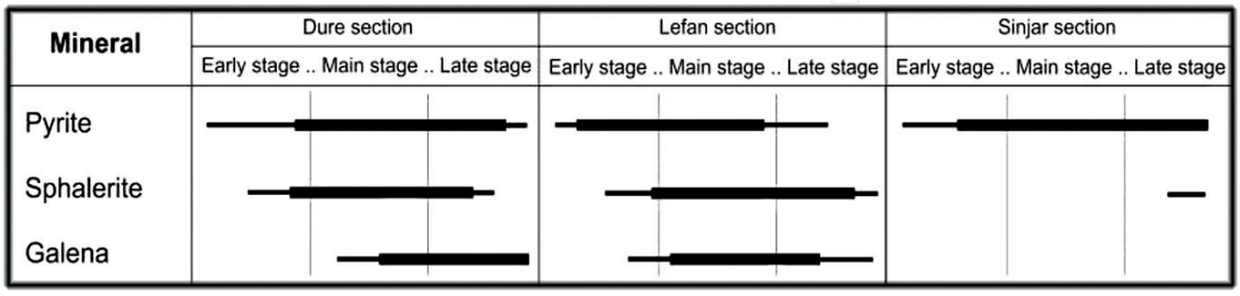

Figure 3. General paragenetic sequence of the sulfide ore deposits in the studied sections (Dure, Lefan, and Sinjar).

Galena in **Table 5** reveals also some impurities as traces in Pb site. At Dure, $Fe_{.001}$ and $Zn_{.001–.003}$ in the main stage are recorded in pyrite, while in the late stage, $Fe_{.003–.29}$, $Zn_{.047–.173}$, and $Cd_{.003–.005}$ as traces in Pb site of pyrite are recorded.

At Lefan, galena has traces of $Zn_{.011–.081}$, $Fe_{.001–.002}$, and $Cd_{.004}$ in the only main stage. No galena is recorded at Sinjar.

5. Paragenesis

Generally, fluid inclusion and stable isotope data constrain the different stages of the rock evolution [9].

5.1. Fluid inclusions

Most fluid inclusions are essentially composed of a liquid phase and/or a vapor bubble, but they may also contain soluble salts and slightly ore elements.

In **Table 7**, the homogenization temperatures are measured for 22 fluid inclusions in sphalerite, dolomite, and calcite minerals from the Dure deposits and 13 fluid inclusions in dolomite and calcite minerals from the Lefan deposits are given. This is helpful to constrain the hydrothermal fluid conditions during the formation of these deposits and to find out evidence of boiling. No suitable sample has been examined from Sinjar deposit for analysis [10].

The Dure deposit contains two phases of fluid inclusions at room temperature. They are H_2O-rich liquid with H_2O vapor bubbles constituting typically 5–10% vapor volume.

Primary fluid inclusions occur as single or clustered rounded or irregular shape inclusions that are ranging in size from 5 μm to < 10 μm (**Figure 4A**). Negative crystal forms are uncommon. Few primary inclusions have vapor volumes greater than 15% (**Figure 4A**). Secondary fluid inclusions occur as fracture-controlled planar groups, and they are thin, elongated, and irregular in shape (**Figure 4B**). The inclusions are <5 μm in size.

At room temperature, the Lefan deposit contains liquid-rich and vapor-rich fluid inclusions. The fluid inclusions typically contain H_2O-rich liquid with H_2O vapor bubbles. Some fluid inclusions contain CO_2 vapor. Vapor-rich inclusions are subrounded or irregularly shaped and occur as clusters containing one to three inclusions (**Figure 4C**). These inclusions are larger in size, 5–12 μm, than the liquid-rich inclusions, <5μm.

Primary fluid inclusions are irregular or rounded and randomly distributed in carbonate minerals (**Figure 4D**). Secondary fluid inclusions form as planar groups of elongated inclusions (**Figure 4E**). The presence of fluid inclusions with variable liquid to vapor volumetric phase ratios is the most common evidence of entrapment from boiling fluids [11]. The vapor-rich inclusions are believed to result from boiling fluids rather than necking-down processes (**Figure 4F**) due to their large size relative to the liquid-rich inclusions. There are absence of one-phase liquid inclusions and the presence of fluid-rich inclusions with relatively constant liquid:vapor phase ratios and consistent Th. The occurrence of vapor-rich and liquid-rich

Sample no.	T_m (°C) Ice melting temperature	T_h (°C) Homogenization temperature	Salinity wt% NaCl equivalent	Origin	Mineral
DO 35					
1	−14.1	174	17.79	Primary	Sphalerite
2	−14.3	173	17.96	Primary	Sphalerite
3	−13.8	183	17.61	Primary	Sphalerite
4		180		Secondary	Sphalerite
5		177		Secondary	Sphalerite
6		179		Secondary	Sphalerite
7		165		Secondary	Sphalerite
8		157		Secondary	Sphalerite
DO 28					
1	−29.1	144	>23	Primary	Saddle dolomite
2	−23.2	147	>23	Primary	Saddle dolomite
3	−18.1	128	20.97	Primary	Saddle dolomite
4		115		Secondary	Saddle dolomite
5		117		Secondary	Saddle dolomite
6		97		Secondary	Saddle dolomite
7		127		Secondary	Saddle dolomite
LO 15					
1	−5.3	284	8.14	Primary	Saddle dolomite
2	−3.2	200	5.11	Primary	Saddle dolomite
2	−5.3	196	8.14	Primary	Saddle dolomite
4	−6.9	210	10.36	Primary	Saddle dolomite
5	−2.2	238	3.55	Primary	Saddle dolomite
6	−1.8	225	3.06	Primary	Saddle dolomite
7		193		Secondary	Saddle dolomite
8		196		Secondary	Saddle dolomite
DO 10					
1	−10.1	61	13.93	Primary	Calcite vein
2	−33.2	59	>23	Primary	Calcite vein
3	−35.1	105	>23	Primary	Calcite vein
4		45		Secondary	Calcite vein
5		50		Secondary	Calcite vein
6		65		Secondary	Calcite vein
7		74		Secondary	Calcite vein

Sample no.	T_m (°C) Ice melting temperature	T_h (°C) Homogenization temperature	Salinity wt% NaCl equivalent	Origin	Mineral
LO 10					
1	−7.8	127	11.46	Primary	Calcite vein
2	−10.2	145	10.04	Primary	Calcite vein
3	−10.6	157	14.57	Primary	Calcite vein
4		71		Secondary	Calcite vein
5		68		Secondary	Calcite vein

Table 7. Homogenization temperatures and salinities of fluid inclusions in sphalerite and carbonate minerals from the Dure (DO-sample) and Lefan (LO-sample) deposits.

inclusions suggests the presence of two immiscible phases due to boiling at the time that the fluid inclusions were trapped. Textures indicative of boiling are present in the Lefan deposit, but are not as common as those cited in other epithermal systems (e.g., Dure section).

5.2. Microthermometric analysis

Microthermometric analyses have been carried out on fluid inclusions in sphalerite, dolomites, and calcites to obtain a preliminary estimate of the temperatures and salinities of the ore-bearing fluid. The results of the microthermometric analyses are summarized in **Table 7**. Suitable fluid inclusions are observed only in saddle dolomite and calcite. Few suitable fluid inclusions are identified in sphalerite, where the observed inclusions are either too small for microthermometric measurement or they are judged to be secondary (**Figure 4A**).

Most inclusions chosen for analyses are considered as primary (contemporaneous with their host minerals) and closely related spatially and genetically to the sulfide mineralization. These inclusions are generally small (about 5 μm) and contain no daughter minerals (**Figure 4A, C,** and **D**). Due to the small size of the inclusions, proving accurate geothermometry is difficult. In addition, some hydrocarbon-rich fluid inclusions are also found in gangue minerals. Fluid inclusions in the late-generated barite within Bekhme formation at Lefan lead-zinc deposit are considered as fingerprint of hydrocarbon generation [3].

Salinities of fluid inclusions are determined by measuring the freezing temperatures of the fluid inclusions. According to Bodnar and Vityk [12], the freezing point of a fluid inclusion is the temperature at which the last ice crystal melts (ice melting temperature). The equation used to determine the salinity of a fluid inclusion is based on the H_2O-NaCI system following Bodnar and Vityk [12].

$$\text{Salinity} = 0.00 + 1.78\theta – 0.0442\theta 2 + 0.00055703 \quad (1)$$

where salinity = the weight percent (wt %) NaCl in solution and θ = freezing point depression (ice melting temperature) in °C. Freezing temperatures were measured prior to homogenization temperatures to avoid leakage or decrepitation of the fluid inclusions [13].

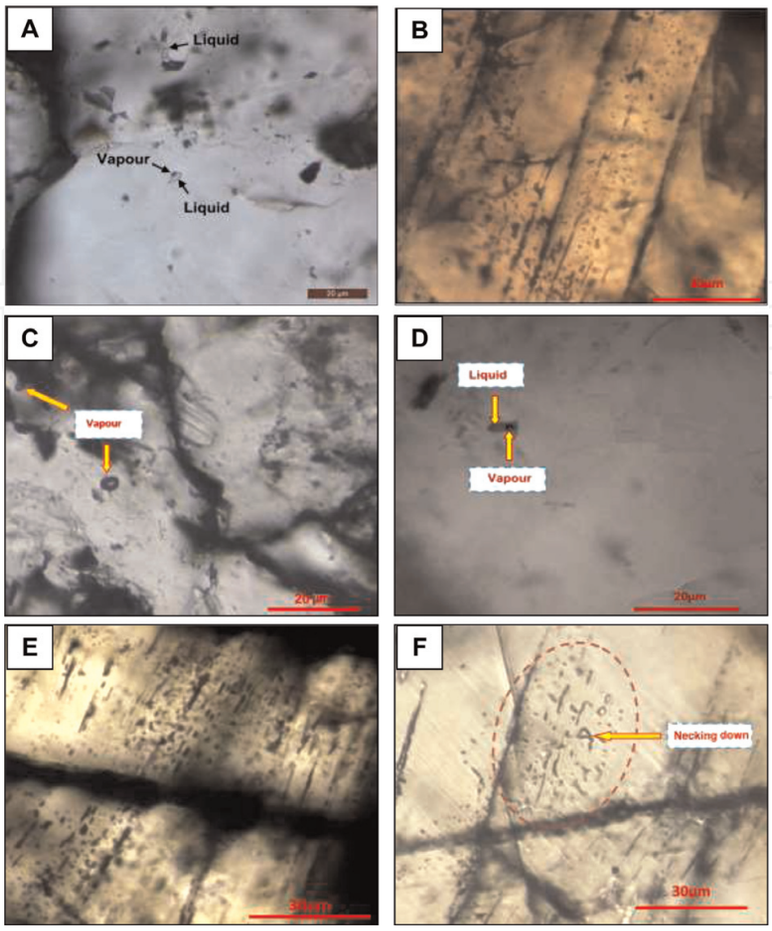

Figure 4. Primary and secondary fluid inclusions from Dure and Lefan lead-zinc deposits. (A) Primary 2-phase fluid inclusion and (B) secondary fluid inclusions within sphalerite (DO 35, Dure section). (C) Primary single-phase vapor inclusions within saddle dolomite (LO 15, Lefan section). (D) Primary two-phase fluid inclusion within calcite (LO 10, Lefan section). (E) Elongated-secondary fluid inclusions within saddle dolomite (LO 15, Lefan section). (F) Necking-down process within saddle dolomite (LO 15, Lefan section). Numbers on scale bars in microns.

The salinities of the fluid inclusions in Dure deposit range from 13.93 to >23 wt% NaCl equivalent, whereas in the Lefan deposit they range from 3.06 to 14.57 wt% NaCl equivalent (**Table 7**).

Homogenization temperatures were determined for primary and secondary inclusions with constant liquid:vapor volumetric phase ratios to avoid inaccurate measurements that could result from necking-down processes, leakage, stretching and decrepitation [11]. Homogenization temperatures of the fluid inclusions in Dure deposit range from 45°C to 183°C, whereas the Lefan deposit has fluid inclusions that homogenize at temperatures ranging from 68°C to 284°C (**Table 7**).

Both Dure and Lefan deposits have relatively some differences in fluid inclusion homogenization temperatures. The primary fluid inclusions in the Dure and Lefan deposits yielded homogenization temperatures with an average value of 130.4°C and 198°C, respectively, although values range from approximately 60°C to 284°C for both sections (**Table 7**).

5.3. Interpretation of fluid inclusion results

The homogenization temperatures and salinities obtained for fluid inclusions in the present study are nearly similar to those reported for lead-zinc deposits of Mississippi Valley Type (MVT). Many authors such as Leach and Sangster [14], Paradis et al. [15], and Leach et al. [16, 17] have given the fluid inclusion temperatures in MVT deposits to range from about 50°C to 250°C; however, most of the measured temperatures were between 75°C and 200°C. The salinities of MVT fluids determined by those authors from fluid inclusions are typically 10–30 wt.% NaCl equivalent.

Both primary and secondary fluid inclusions of the deposits at Dure area contain the lowest Th values when compared to those of the Lefan area. The Lefan deposits have some vapor-rich fluid inclusions homogenized at relatively higher temperatures (200–280°C). These anomalous high temperatures can probably attributed to a vapor-rich fluid that trapped some liquid during boiling. During crystallization of sphalerite, the high temperature was preceded, but relatively moderate formation temperatures during the formation of saddle dolomite followed by cooling to about 50°C for late calcite formation. This supports the hypothesis of dilution and cooling of the transmitted fluids in the cracks and fissures of the host rocks by mixing with meteoric waters during later formed sulfides or perhaps post-sulfide calcite stages of deposition.

The diagram of salinity versus homogenization temperature of the fluid inclusions in the studied sections reveals no limit relationship (**Figure 5**), but rather scattered between inclusion salinities and homogenization temperatures. This may be due to mixing of two different solutions; one was hot and saline, and the other was cool with low salinity (e.g., Taylor et al. [18]) as in Lefan section. Furthermore, invariant salinities of inclusions are interpreted as evidence of precipitation from a single fluid [19], as in Dure section.

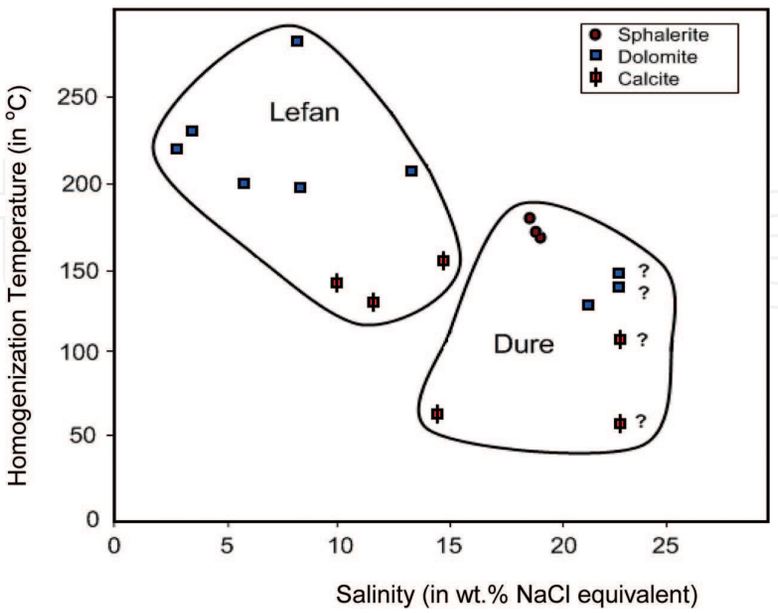

Figure 5. Fluid inclusion salinity vs. homogenization temperature for the studied deposits (Dure and Lefan sections). Question mark means that the absolute value of salinity is not determined (i.e., >23%).

Accordingly, the mineralization of the studied sulfides is seen to follow the type of MVT mineralization. However, the similarities between MVT inclusion fluids and oil-field brines are established to a wide acceptance of a basin-generated origin for MVT fluids. The high salinity is explained by the dissolution of evaporites, incorporation of connate bittern brines, or through infiltration of evaporated surface waters of the sedimentary basin brines [16, 17, 20].

5.4. Genesis of sulfides from stable isotopes

The average values of $\delta^{34}S‰$ of the studied sulfide of Dure, Lefan, and Sinjar are (0.8, 1.8, and 30.8‰), respectively. Sulfur isotope analysis shows that the sulfur in Dure and Lefan is originated from a mixture of various sources, but probably derived from seawater dissolved sulfate and/or diagenetic pyrite for Sinjar deposits. The $\delta^{13}C$ and $\delta^{18}O$ values of carbonate-host rocks are in the range of marine carbonates. Petrographic evidence and stable isotope data with fluid inclusions suggest that lead-zinc mineralization was caused by deeply circulating mineralizing fluids of high temperature (brines) within the source basin of deposition or due to tectonic processes, which possibly contribute in leaching metals from either the diagenetic host rocks or dewatering of deeper buried siliciclastic beds. The studied carbonate-hosted lead-zinc deposits seem to have many similarities with Mississippi Valley Type (MVT) deposit.

Deposit locality	Sample	Mineral	$\delta^{34}S$ ‰	Author(s)
Dure	DO 25	Pyrite	0.9	Present study
	DO 22	Pyrite	1.3	Present study
	DO 15	Pyrite	1.6	Present study
		Pyrite	0.2	Al-Bassam et al. [1]
		Pyrite	3.6	Al-Bassam et al. [1]
	DO 22	Sphalerite	2.4	Present study
	DO 30	Sphalerite	2.0	Present study
		Sphalerite	0.0	Al-Bassam et al. [1]
		Sphalerite	−0.4	Al-Bassam et al. [1]
	DO 28	Galena	1.8	Present study
	DO 30	Galena	−0.9	Present study
		Galena	−1.8	Al-Bassam et al. [1]
		Galena	−2.6	Al-Bassam et al. [1]
Lefan	LO 22	Pyrite	3.6	Present study
	LO 15	Sphalerite	1.8	Present study
	LO 15	Galena	1.2	Present study
	LO 18	Galena	0.47	Present study

Table 8. Sulfur isotope ($\delta^{34}S$) values of the studied lead-zinc deposits. Data of pyrite (n = 2), sphalerite (n = 2), and galena (n = 2) in Dure deposits from Al-Bassam et al. [1] were also displayed.

http://dx.doi.org/10.5772/intechopen.72483

The values of sulfur isotope in the Dure (average = 0.8‰) and Lefan (average = 1.8‰) (**Table 8**) cannot be attributed necessarily to a magmatic source of sulfur because the field observations together with ore microscopy provide no magmatic activity. The negative shift of $\delta^{34}S$ value is resulted from seawater sulfates, or bacterial reduction, but possibly some sulfur could be derived due to the dissolution and leaching of preexisting sulfide-bearing igneous rocks.

The positive $\delta^{34}S$ values suggest that sulfur was derived from seawater or ancient evaporates and connate water undergone subsequent reduction by ferrous iron or organic compounds [21] (see **Figure 6** for more details). Perhaps seawater became enriched in light isotope by leached sulfur from deeper lithologic units during water circulation [23–25]. The influence of the enrichment of light sulfur isotopes is more significant for the Dure deposits (average, 0.8‰) than that for Lefan (average, 1.8‰).

Previous studies [1, 2, 26], together with this study, assumed that the studied Pb-Zn deposits are epigenetic of sedimentary origin formed after lithification of their host rocks.

Several evidences suggest the basinal brines source for hydrothermal fluids in the studied sections that are responsible for ore formation: first, the salinities and temperatures of the fluid inclusions of these deposits are mainly within the range of fluids of the MVT deposits [16, 17]; Second, the similarity in composition between the ore deposits and the most basinal brines. Low and narrow variation in $\delta^{34}S$ values of sulfides (**Table 9**) may indicate a single source of sulfur. Because of the absence of magmatic activity, it is realistic to consider the rocks in the basin of the studied sections as the source of sulfur. This leads to accept the positive $\delta^{34}S$, the organic sulfur enrichment in the beds of slightly positive to negative $\delta^{34}S$, and the presence of diagenetic pyrite in sedimentary rocks. Third, carbon and oxygen isotope values in the carbonate-host rocks are generally of relatively lower $\delta^{18}O$ and higher $\delta^{13}C$. These values

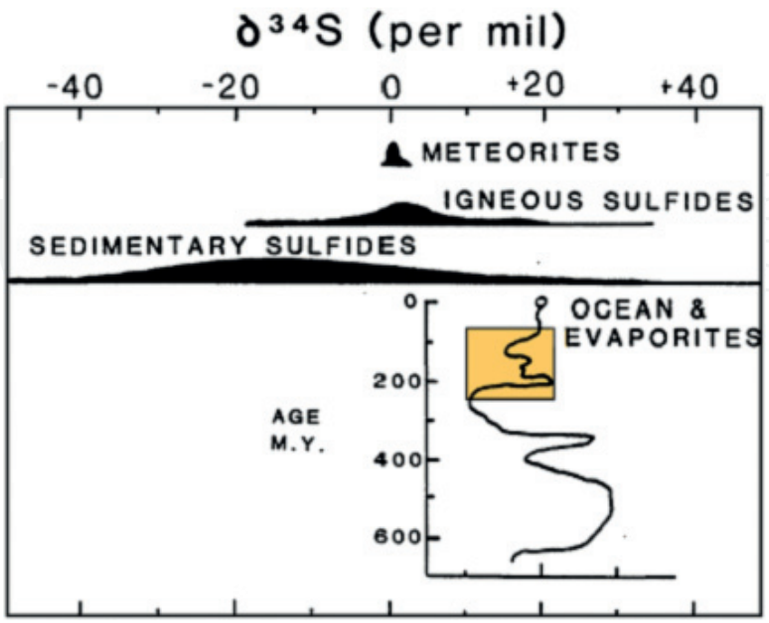

Figure 6. Sulfur isotopic variation in nature (from Ohmoto and Rye [22]).

Sample	Lithology	$\delta^{13}C_{PDB}$ (‰)	$\delta^{18}O_{PDB}$ (‰)	$\delta^{18}O_{SMOW}$ (‰)
DK 90	Dolomitized lime-mudstone	−1.05	−4.48	26.24
DK 84	Black dolomitic shale	0.60	−8.48	22.12
DK 80*	Fine dolomitized limestone	1.23	−7.71	22.91
DK 70*	Brecciated dolostone	1.16	−6.94	23.71
DK 65*	Saddle dolomite	−1.25	−11.93	18.56
DK 58*	Smithsonite ($ZnCO_3$)	−2.77	−10.09	20.46
DK 45	Coarse dolomitized limestone	0.59	−5.49	25.20
DK 32	Coarse gray dolostone	−1.57	−9.01	21.57
DK 25	Bioclastic lime-mudstone	−1.30	−8.70	21.89
DK 18	Brecciated dolomitic limestone	−2.80	−8.48	22.12
DK 10	Bioclastic lime-wackstone	−1.00	−9.01	25.01
LSh 1	Packstone (limestone)	0.31	−4.53	26.19
LB 68	Coarse dolostone	1.93	−8.19	22.42
LB 64	Dolomitized lime-wackstone	−0.41	−5.67	25.01
LB 60	Dolomitized lime-wackstone	2.23	−4.83	25.88
LB 55	Dolomitized lime-wackstone/packstone	1.37	−5.37	25.32
LB 53*	Dolostone with saddle dolomite	−2.53	−7.04	23.61
LB 35*	Dolomitized lime-packstone	1.61	−5.20	25.50
LB 32*	Dolomitized lime-grainstone	0.96	−6.15	24.52
LB 31*	Recrystallized limestone	0.94	−5.93	24.75
LB 28	Dolomitized lime-grainstone	−3.34	−7.13	23.51
LB 25	Dolomitic limestone	1.28	−3.77	26.98
LB 20	Recrystallized lime-wackstone	1.13	−5.91	24.77
LB 17	Dedolomitized dolostone	1.24	−4.87	25.84
LB 12	Rudist boundstone (limestone)	1.27	−3.94	26.80

DK samples from Dure section and LB samples from Lefan section. LSh 1 is one sample from Shiranish formation from Dure section.
*Mineralized samples. Others unmineralized samples.

Table 9. Carbon ($\delta^{13}C$) and oxygen ($\delta^{18}O$) isotope values of carbonate-host rocks.

require involvement of marine carbonates and organic matter in the basin to supply such carbon and oxygen (**Figure 7**). Moreover, there is a fact about the presence of hydrocarbon-rich fluid inclusions in some gangue minerals, and a late generation of barite [3], all supporting the probable basinal brines as the source of ore-forming fluids. As compared with typical basinal brines, some fluid inclusions in the present studied samples exhibit relatively lower salinities (<10 wt.% NaCl equiv.). The low salinity of these fluid inclusions shows a positive correlation with their Th content, possibly due to mixing between meteoric water and basinal brines.

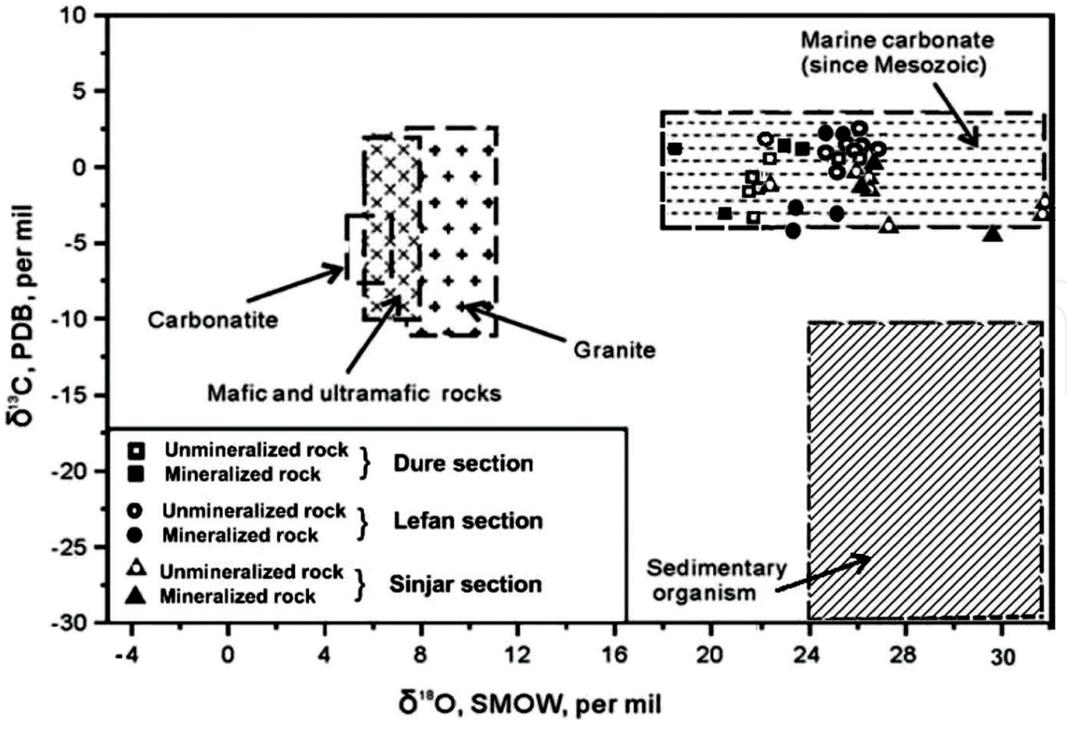

Figure 7. Plot of $\delta^{13}C$ vs. $\delta^{18}O$ of carbonate-host rocks of the studied deposits in the Dure and Lefan sections, showing $\delta^{13}C$ and $\delta^{18}O$ values of the unmineralized and mineralized carbonate rocks in the sections [4]. The fields of carbonatite, mafic and ultramafic rocks, granite, marine carbonate, and sedimentary organisms are after He et al. [27].

6. Conclusions

The geochemical prospect throughout the recognition, characterization, fluid inclusions, and stable isotopes of the studied ore deposits carried out in this study emphasizes the suggestion that the Pb-Zn-Fe mineralization is concentrated from brines (marine waters). It is thought that the circulation of hydrothermal water happened at depths, where cracks and faults were formed at the beginning of the orogeny event. At that depth, the fluid was heated enough to dissolve metals from their hosting rocks during its ascent, and as the transported metal ions concentrated sufficiently, deposition took place. This process, together with permeability of the wall rock, is thought to be the eventual controlling factor of mineralization and the present geometry of the ore bodies and the alteration. Mineralization tends to occur in fractures and solution-collapse features formed during uplift of platform-carbonate sequences accompanying plate convergence. Therefore, the preferred genetic model for the concentration of ore metals at the studied carbonate rocks should involve basin dewatering due to compaction and regional tectonism and expulsion of the basin-derived fluids into the brecciated, karstificated, and highly porous recrystallized and dolomitized host rocks of the Kurra Chine and Bekhme formations.

Acknowledgements

The authors would like to thank the Earth Science Department, College of Science, Mosul University, for supplying available facilities and administrative support. A special thank goes

to Dr Dave Alderton from Royal Holloway, London University, for his help in XRD; Prof. Dr Ahmet Gokce, Cumhuriyet University, Turkey; and Mrs Soheila Aghajani, Iran Mineral Processing Research Center (IMPRC) for their contribution to the fluid inclusion analysis. Considerable gratitude goes to NERC Isotope Community Support Facility, SUERC, Glasgow, Scotland, for sulfur isotope analysis, and to University-College London UCL, UK, for support in electron microprobe analysis (EMPA).

Author details

Ali Ismail Al-Juboury[1]*, Waleed S. Shingaly[2], Elias M. Elias[1] and Mohsin M. Ghazal[1]

*Address all correspondence to: alialjubory@yahoo.com

1 Geology Department, Mosul University, Mosul, Iraq

2 Geology Department, Salahaddin University, Erbil, Iraq

References

[1] Al-Bassam K, Hak J, Watkinson D. Contribution to the origin of the Serguza lead-zinc-pyrite deposit, Northern Iraq, Mineral. Deposita. 1982;**17**:133-149

[2] Awadh SM. Mineralogy, geochemistry and origin of the zinc–lead–barite deposits from selected areas from north of Zakho, Northern Iraq [thesis]. Iraq: University of Baghdad; 2006

[3] Awadh SM, Al-Ameri TK, Jassim SY, Bayraktutan MS. Fluid inclusions usage for assessing oil migration in Duhok, north Iraq. Positioning. 2010;**1**:42-49

[4] Shingaly WSA. The role of carbonate host rocks in the genesis of lead-zinc sulfide deposits at Dure and Lefan sections and iron-sulfide deposit at Sinjar Section-Northern Iraq [thesis]. Iraq: Mosul University; 2013

[5] Sharland PR, Archer R, Casey D, et al. Arabian Plate Sequence Stratigrpahy, GeoArabia, Special Publication 2, Gulf Petrolik. Manama, Bahrain; 2001. 371 p

[6] Bellen RC, van Dunnington HV, Wetzel R, Morton DM. Lexique stratigraphique international. Asie, Iraq: International Geology Congress Commission de Stratigraphique, Fasco.10a. 1959;**3**:333

[7] Buday T. The regional geology of Iraq. Stratigraphy and Paleogeography. Dar Al-Kutub pub. University of Mosul, Iraq. 1980:**1**:445

[8] Jassim SZ, Goff, JC. Geology of Iraq, Published by Dolin, Prague and Moravian Museum, Brno. Printed in the Czech Republic. 2006. 341 p

[9] Van den-Kerkhof AM, Hein UF. Fluid inclusion petrography. In: Andersen T, Frezzotti ML, Burke EA, editors. Fluid Inclusions: Phase Relationships-methods-applications (Special Issue). Lithos. 2001;**55**(1-4):320

[10] Shingaly WS, Al-Juboury AI, Elias ME. The role of carbonate-host rocks on the genesis of lead-zinc deposits in Kurdistan Region, Northern Iraq. Journal of Tethys. 2015;**3**(1):31-47

[11] Bodnar RJ, Reynolds TJ, Kuehn CA. Fluid inclusion systematics in epithermal systems. In: Berger BR, Bethke PM, editors. Reviews in economic geology: geology and geochemistry of epithermal systems. Society of Economic Geologists. 1985;**2**:73-97

[12] Bodnar RJ, Vityk MO. Interpretation of microthermometric data for H_2O-NaCl fluid inclusions. In: De Vivo B, Frezzotti ML, editors. Fluid Inclusions in Minerals: Methods and Applications. Blacksburg: Virginia Technical Publication; 1994. pp. 117-130

[13] Roedder E. Fluid Inclusions, Mineralogical Society of America, Reviews in Mineralogy; 1984;**12**:644

[14] Leach DL, Sangster DF. Mississippi valley-type lead–zinc deposits. In: Kirkham RV, Sinclair WD, Thorpe RI Duke JM, editors. Mineral Deposit Modeling. Geological Association of Canada, Special Paper; 1993;**40**:289-314

[15] Paradis S, Hannigan P, Dewing K. Mississippi Valley-Type lead-zinc deposits. In: Goodfellow WD, editor. Mineral Deposits of Canada: A Synthesis of Major Deposit-types, District Metallogeny, the Evolution of Geological Provinces, and Exploration Methods. Geological Association of Canada, Mineral Deposits Division. 2007;**5**:185-203

[16] Leach DL, Sangster DF, Kelly KD, Large RR, Garven G, Allen CR, Gutzmer J, Walters S. Sediment-hosted lead–zinc deposits: A global perspective. Economic Geology. 2005;**100th** Anniversary Volume:561-607

[17] Leach DL, Taylor RD, Fey DL, Diehl SF, Saltus RW. A Deposit Model for Mississippi Valley-Type Lead-Zinc Ores, Chapter A of Mineral Deposit Models for Resource Assessment, USGS, Sci. Inv. Report 5070A. 2010. 52 p

[18] Taylor M, Kesler SE, Cloke PL, Kelly WC. Fluid inclusion evidence for fluid mixing, Mascot-Jefferson City zinc district, Tennessee. Economic Geology. 1983;**78**:1425-1439

[19] Gratz JF, Misra KC. Fluid inclusion study of the Gordonsville zinc deposit, central Tennessee. Economic Geology. 1987;**82**:1790-1804

[20] Hanor JS. The sedimentary genesis of hydrothermal fluids. In: Barnes HL, editor. Geochemistry of Hydrothennal ore Deposits. New York: Wiley Inter-science; 1979. pp. 137-142

[21] Schütfort EG. The Genesis of the San Vicente Lead Zinc Rhythmite Deposit, Peru—A Petrologic, Geochemical, and Sulfur Isotope Study [thesis]. USA: Oregon State University; 2001

[22] Ohmoto H, Rye RO. Isotopes of sulphur and carbon. In: Barnes HL, editor. Geochemistry of Hydrothermal Ore Deposits. New York: Wiley-Interscience; 1979. pp. 509-567

[23] Eldridge CS, Williams N, Walshe JL. Sulfur isotope variability in sediment-hosted massive sulfide deposits as determined using the ion microprobe SHRIMP: II. A study of the H.Y.C. deposit at McArthur river, Northern Territory, Australia. Economic Geology. 1993;**88**:1-26

[24] Sherlock RL, Roth T, Spooner ET, Bray CJ. Origin of the Eskay Creek precious metal-rich volcanogenic massive sulfide deposit: Fluid inclusion and stable isotope evidence. Economic Geology. 1999;**94**:803-824

[25] Roth T, Taylor BE. Sulfur isotope and textural zoning of pyrite in mudstone about the polymetallic Eskay Creek Deposit, Northwestern British Columbia, Canada. In: Volcanic Environments and Massive Sulfide Deposits International Conference; Hobart, Tasmania. 2000. pp. 16-19

[26] Al-Qaraghuli N, Lang H. Geochemical and mineralogical investigation of pyrite-sphalerite-galena deposit in Duri-Serguza area, Northern Iraq. Geological Society of Iraq. 1978;**11**:46-66

[27] He L, Song Y, Chen K, Hou Z, Yu F, Yang Z, Wei J, Li Z, Liu Y. Thrust-controlled, sediment-hosted, Himalayan Zn–Pb–Cu–Ag deposits in the Lanping foreland fold belt, eastern margin of Tibetan Plateau. Ore Geology Reviews. 2009;**36**:106-132